RSC Advances

PAPER

View Article Online
View Journal | View Issue

Cite this: *RSC Adv.*, 2020, **10**, 45028

Self-dispersible graphene quantum dots in ethylene glycol for direct absorption-based medium-temperature solar-thermal harvesting†

Ruiming Lin, Jingyi Zhang, Lei Shu, Jing Zhu, Benwei Fu, Chengyi Song, Wen Shang, Peng Tao* and Tao Deng*

Received 23rd September 2020
Accepted 1st December 2020

DOI: 10.1039/d0ra08128k

rsc.li/rsc-advances

Poor dispersion stability of carbon nanofluids is one of the key issues limiting their solar-thermal applications especially under medium-to-high temperatures. Herein, this work reported a facile way to prepare stably dispersed graphene quantum dot-ethylene glycol (GQD-EG) medium-temperature solar-thermal nanofluids. The hydroxyl-terminated GQDs were synthesized by a scalable hydrothermal approach. The obtained GQDs have a small particle size, narrow particle size distribution and are self-dispersible within EG fluids. The GQD-EG nanofluids maintained their uniform dispersion after continuous heating at 180 °C for 7 days. The hydrogen bonding between the hydroxyl group on the surface of GQDs and the EG molecules helped achieve homogenous dispersion of GQDs in the nanofluids, and the small particle size and low density of GQDs helped mitigate the sedimentation tendency. The dispersed GQD-EG nanofluids have demonstrated broadband absorption of sunlight, high specific heat capacity and low viscosity, which are all desired for high-performance direct absorption-based solar-thermal energy. The prepared GQD-EG nanofluids have exhibited consistent volumetric harvesting of solar-thermal energy under concentrated solar illumination with a heating temperature up to 170 °C.

Introduction

Conversion of sunlight into storable heat is an attractive way to harness abundant solar energy due to the high energy conversion efficiency, cost-effectiveness, and environmental compatibility.[1–3] In recent years, great efforts have been devoted to the exploration of the harvested solar-thermal energy for high-efficiency interfacial evaporation,[3] desalination,[4–6] clean water generation,[7] domestic and industrial heating,[8] thermotherapy[9,10] and many other important applications.[11] The collected solar-thermal energy can be further converted into electricity through thermoelectric conversion.[12,13] Efficient and facile harvesting of solar-thermal energy is critical to overcome solar intermittency and realize continuous operation of the aforementioned processes. Direct absorption-based solar collectors (DASCs), which utilize homogeneously distributed optical nanofluids to absorb incident sunlight and convert it into heat, have emerged as a superior device to conventional surface absorption-based collectors for solar-thermal energy harvesting.[14,15] In conventional surface absorption-based collectors, solar-thermal energy is harvested by a surface coating and the converted heat is then transferred into the working fluids within the collector. Such configuration causes a large thermal resistance between the absorber surface and working fluids, which results in heat accumulation near the surface of the absorber. By contrast, the volumetric solar-thermal conversion within the working fluids avoids the long-distance heat transfer, thus DASCs have more uniform temperature distribution, minimize surface heat loss and achieve high solar-thermal harvesting efficiency. A critical requirement of DASC is that the nanofluids can volumetrically absorb the incident sunlight.[16] Carbon nanomaterials can efficiently absorb the broad-spectrum sunlight and have good chemical stability, thus graphite nanofluids,[17] carbon nanotube nanofluids[18,19] and graphene nanofluids[16] have received intensive research attention for the DASC application. To date, most of the investigated carbon nanofluids are water-based and they are used for low-temperature solar-thermal energy harvesting. By comparison, medium-temperature solar-thermal energy (80–250 °C) can provide more intensive heating for a broad range of applications such as steam generation, sterilization, cooking and industrial process heating.[8] Under the elevated operation temperatures, however, the nanoscale solar absorbers have stronger tendency to lose their uniform dispersion within the nanofluids.[20,21] The carbon solar absorbers tend to aggregate and precipitate out of the nanofluids, which will lose the volumetric absorption of sunlight and even cause blockage of the DASC.[22] To improve the dispersion stability of the nanofluids, surface modification of solar absorbers with surfactants, organic ligands or polymer

State Key Laboratory of Metal Matrix Composites, School of Materials Science and Engineering, Shanghai Jiao Tong University, Shanghai, 200240, China. E-mail: taopeng@sjtu.edu.cn; dengtao@sjtu.edu.cn

† Electronic supplementary information (ESI) available. See DOI: 10.1039/d0ra08128k

chains is usually required, which adds both fabrication complexity and cost to the solar-thermal nanofluids.[23,24] Therefore, developing self-dispersible medium-temperature carbon solar-thermal nanofluids, which at best can be prepared through a facile way at large scale, is still a grand challenge.

In the family of carbon derivatives, graphene quantum dots (GQDs) are graphene nanoparticles consisting of one or a few graphene layers along the thickness direction and have a lateral size smaller than 100 nm.[25] In recent years, GQDs have received extensive research interest due to its small size,[26] unique spin,[27] photoluminescence[28] and electronic properties.[29] These fascinating physical and chemical properties provide vast opportunities to explore bioimaging,[30] photodetection,[31] light emission,[32] electrocatalysis[33] and electrical energy harvesting applications.[34] Thanks to the broad light absorption from ultraviolet to the visible light region and the outstanding photostability,[35] GQDs also hold great potential for solar energy harvesting, conversion and utilization.[36] Current solar related applications of GQDs mainly focus on photovoltaics and photocatalysis.[37–39] However, the exploration on employing GQDs to prepare self-dispersible solar-thermal nanofluids for medium-temperature solar-thermal energy harvesting has not been reported.

In this work, we report the preparation of stably-dispersed GQDs nanofluids for direct absorption-based solar-thermal energy harvesting at medium temperatures. Gram-scale hydroxyl-functionalized graphene quantum dots (OH-GQDs) were synthesized through a single-step hydrothermal reaction. The obtained OH-GQDs are self-dispersible within commercial medium-temperature ethylene glycol (EG) heat transfer fluid. Dispersion stability tests show that the resultant GQD-EG nanofluids can maintain the uniform dispersion under continuous heating at 180 °C for 7 days. Theoretical analyses indicate that the ultrasmall particle size helped effectively suppress the interparticle van der Waals attraction, and the hydrogen bonding between the surface hydroxyl groups and the EG molecules promotes the formation of homogenous dispersion. The small mass of individual GQD significantly lowers the sedimentation velocity such that it can be counterbalanced by the thermal Brownian motion, which in turn ensures the long-term dispersion stability of the GQD-EG nanofluids. In addition, the GQD-EG nanofluids have demonstrated high solar absorptance, large specific heat capacity and low viscosity. Repeated direct absorption solar-thermal energy harvesting tests show that the GQD-EG nanofluids can efficiently and consistently convert concentrated solar illumination into storable heat with a temperature up to 170 °C. It is anticipated that the development of self-dispersed GQD-EG nanofluids will help accelerate the practical applications of solar-thermal technologies toward higher temperature ranges.

Materials and methods

Materials

Pyrene ($C_{16}H_{10}$) was purchased from Tokyo Chemical Industry Co., Ltd. Nitric acid, sodium hydroxide (NaOH) and EG were purchased from Sinopharm Chemical Reagent Co., Ltd. All reagents were used as received.

Synthesis of OH-GQDs

OH-GQDs were synthesized by a bottom-up method following the procedure reported by Wang *et al.*[40] Typically, 0.5 g pyrene and 40 mL of concentrated nitric acid were added into a 200 mL round flask. The reactants were placed at 80 °C under stirring and refluxing for 12 h. After cooling down to room temperature, the suspension was diluted with 250 mL of deionized (DI) water and filtered through a 0.22 μm microporous membrane to remove the acid. The as-synthesized 1,3,6-trinitropyrene was dispersed in 100 mL of 0.2 M aqueous NaOH solution by ultrasonication. The mixture was then transferred to a Teflon autoclave, which was placed within an oven at 200 °C for 10 h. After the hydrothermal treatment, the suspension was filtered through a 0.22 μm microporous membrane to remove the insoluble products, and further dialyzed in a dialysis bag for 2 days. The OH-GQDs were obtained by drying the solution within an oven at 70 °C for 24 h.

Preparation of solar-thermal fluids

The OH-GQDs were added into ethylene glycol, followed by mechanical mixing with a glass rod and ultrasonication (200 W, 40 kHz) for 30 min. The dispersed fluids were then transferred to a Teflon autoclave and heated at 180 °C for 6 h. The final GQD-EG solar-thermal fluids were obtained by cooling the dispersion to room temperature.

Characterization and property measurement

The morphology and particle size distribution of GQDs were observed with a transmission electron microscope (TEM, FEI Talos F200X) operated at 200 kV. The particle size distribution was analyzed by Image J software through counting more than 100 GQD particles for each sample. Atomic force microscope (AFM, Bruker Multimode Nanoscope V) was used to analyze the thickness of GQDs. The surface functional groups on GQDs were probed by a Fourier transform infrared spectrometer (FTIR, Nicolet 6700) and the X-ray photoelectron spectrometer (XPS, AXIS UltraDLD). Optical transmission and absorption spectra of solar-thermal fluids were measured at room temperature by a UV-Vis spectrometer (PerkinElmer Lambda 330). The specific heat capacity was tested by a differential scanning calorimeter (DSC, PerkinElmer DSC8000, TA Instruments) through raising the temperature from 12 °C to 110 °C at the rate of 10 °C min^{-1}. The viscosity of each sample was measured by a viscometer (Fangrui, LVDV-1T). A dynamic light scattering apparatus (DLS, Malvern, Zetasizer Nano ZS) was used to measure the hydrodynamic size of GQD. Zeta potential (ζ) of the solar-thermal fluids was measured by the Particle Sizer and Zeta Potential Analyzer (Omni Instruments, Japan). The thermal conductivity of EG and GQD-EG nanofluids was measured by a thermal conductivity meter (Hot Disk TPS 2500 S) with a heating power of 80 mW.

Results and discussion

Preparation and characterization of solar-thermal fluids

As shown in Fig. 1a, instead of applying the top-down synthetic routes that cut large graphene sheets into GQDs,[41,42] herein

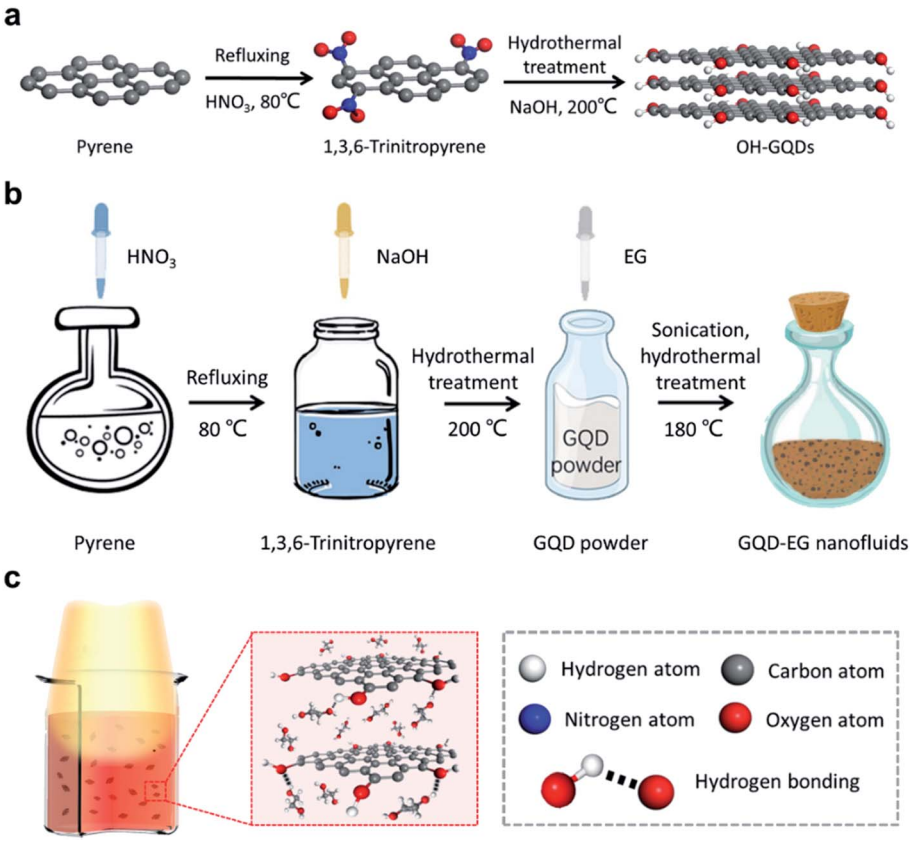

Fig. 1 (a) Synthetic procedure of OH-GQDs. (b) Schematic fabrication process of GQD-EG nanofluids. (c) Homogeneously dispersed GQD-EG nanofluids for direct absorption-based solar-thermal energy harvesting.

a bottom-up method was adopted and pyrene was used as the precursor. In general, the bottom-up method has better control of particle size and surface chemistry than the top-down approaches, which is highly desired for engineering their dispersion in nanofluids. Gram-scale of high-quality GQDs could be readily produced through such route each time under mild hydrothermal conditions. Fig. 1b shows that pyrene was first nitrated into yellow 1,3,6-trinitropyrene, following by the hydrothermal treatment in NaOH aqueous solution to further transform the sample into black OH-GQDs.

It was found that the obtained OH-GQD powders can be mixed with the EG base fluid at room temperature through mechanical agitation. With further ultra-sonication, the GQD-EG nanofluids seem to be well-dispersed. However, the DLS measurement shows that there are still some big particles in the fluids (Table S1†). The existence of big agglomerates implies that at room temperature mechanical and ultrasonic agitation cannot effectively break the centrifuged GQD powders into homogeneously dispersed particles. To tackle this problem, further hydrothermal treatment was carried out by placing the GQD-EG nanofluids within a Teflon autoclave and heating it within an oven at 180 °C for 6 h. At the elevated temperature, EG molecules can more easily diffuse into the GQD powders and interact with the surfaces of GQDs, thus promoting the separation of the bulk GQD powders toward nanoparticles. Due to the favorable interaction between the polar EG molecules and the hydroxyl groups on the surfaces, the prepared OH-GQDs are self-dispersible in the EG base fluid (Fig. 1c). The hydrothermal treatment also helps prescreen dispersion stability of the solar-thermal nanofluids and stable dispersion can be anticipated when the application temperature is slightly lower than the treatment temperature (180 °C).

TEM observation in Fig. 2a shows that the OH-GQDs have a small plate morphology, and a narrow lateral particle size distribution (8.0 ± 1.9 nm, Fig. 2b). The HRTEM image in Fig. 2c shows the single crystal structure for the OH-GQDs with an interplanar crystal spacing of 0.21 nm, which is further confirmed by the periodically oscillating intensity profile (Fig. S1†). The AFM image in Fig. 2d also shows uniform distribution of the drop-casted OH-GQDs on the Si wafer after solvent evaporation. The thickness of OH-GQDs was measured to be in the range of 0.5–2.5 nm, which corresponds to 1 to 5 graphene layers. The FTIR spectra in Fig. 2e show the C–H stretching vibrations from the sp^2 hybridized carbon atoms in the range of 3000–3100 cm^{-1} for pyrene.[43] After nitration, strong characteristic spectra of N–O bonds were observed in the range of 1250–1500 cm^{-1}. For the OH-GQDs, peaks corresponding to strong and broad vibration of O–H bonds in the range of 3200–3600 cm^{-1} were observed. XPS measurement of pyrene shows a strong peak of C 1s at 284.8 eV (Fig. 2f). The XPS spectrum of OH-GQDs in Fig. 2g shows strong signals of C 1s and O 1s at 531 eV and a weak signal from the sodium impurity at 496 eV. There is

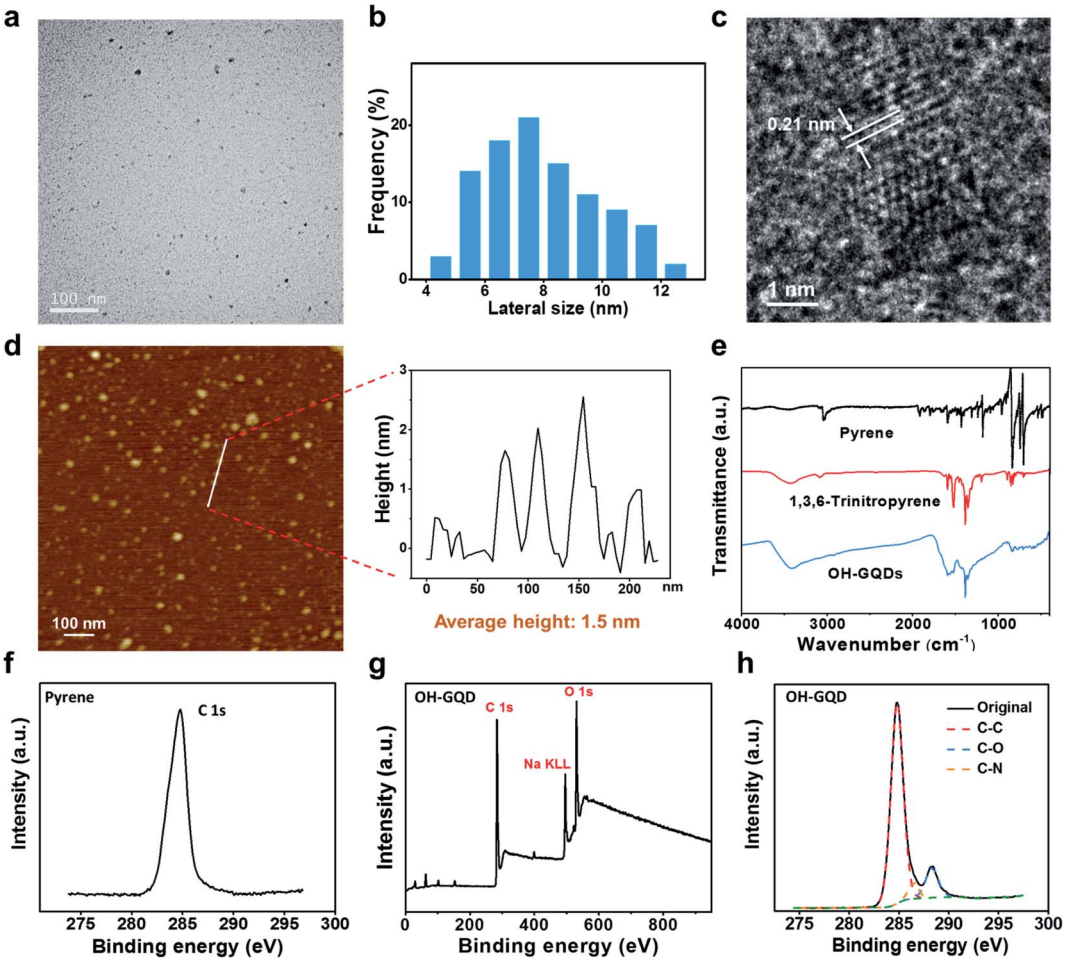

Fig. 2 (a) TEM image of OH-GQDs. (b) Particle size distribution profile of as-synthesized OH-GQDs. (c) HRTEM image of OH-GQDs. (d) AFM image of OH-GQDs (right: scanning height profile along the white line). (e) FTIR spectra of pyrene, 1,3,6-trinitropyrene and OH-GQDs. (f) XPS C 1s curve of pyrene. (g) XPS spectrum of OH-GQDs. (h) XPS C 1s curve of OH-GQDs.

also a weak signal of N 1s at 399 eV. The C 1s curve (Fig. 2h) presents strong peaks of C=C and C–O bonds indicating the formation of –OH groups on the surface of GQDs. The significantly weakened C–N bonds indicate that 1,3,6-trinitropyrene has been fused into OH-GQDs and the $-NO_2$ groups were removed under the strong alkaline hydrothermal treatment.

Dispersion stability test and analysis

Maintaining homogeneous dispersion of the nanofluids is a prerequisite to pursue direct absorption-based volumetric solar energy harvesting. The dispersion stability of GQDs within EG was evaluated by optical absorption measurement. Fig. S2† shows that the absorption spectra of the GQD-EG nanofluids with three different loadings (0.05 mg mL^{-1}, 0.1 mg mL^{-1}, 0.2 mg mL^{-1}) and different storage time (as-prepared, 14 days and 1 month) are almost coincident with each other, which also indicates the stable dispersion of the nanofluids at room temperature. The medium-temperature dispersion stability was tested by continuously heating the GQD-EG nanofluids at 180 °C for 12 h and 7 days, respectively. Fig. 3a shows that the nanofluids have retained the homogenous dispersed appearance after heating at 180 °C for 7 days. TEM observation indicates that the GQDs have maintained their morphology and no agglomeration was observed after the long-time heating tests (Fig. 3b). The TEM particle size distribution histograms in Fig. 3c show the lateral size of OH-GQDs has largely maintained same (7.5 ± 2.1 nm) after the heating tests. DLS measurement also shows that the hydrodynamic diameter of GQDs has negligible difference before and after the heating tests (Fig. 3d). The stable dispersion state of GQD-EG nanofluids was also checked by the optical spectrum measurement. Fig. 3e presents that the optical absorption spectra of the nanofluids after heating for 12 h and 7 days are almost overlapped with the as-prepared ones. The zeta potential measurement indicates that the GQD-EG nanofluids have retained an absolute zeta potential larger than 30 mV before and after the heating tests, which resists the aggregation and ensures the uniform dispersion of GQDs in EG (Table S2†).

Theoretically, in order to achieve stable dispersion during the long-term heating tests, both aggregation tendency and sedimentation tendency of the GQDs need to be suppressed. The aggregation tendency is governed by the relative strength of

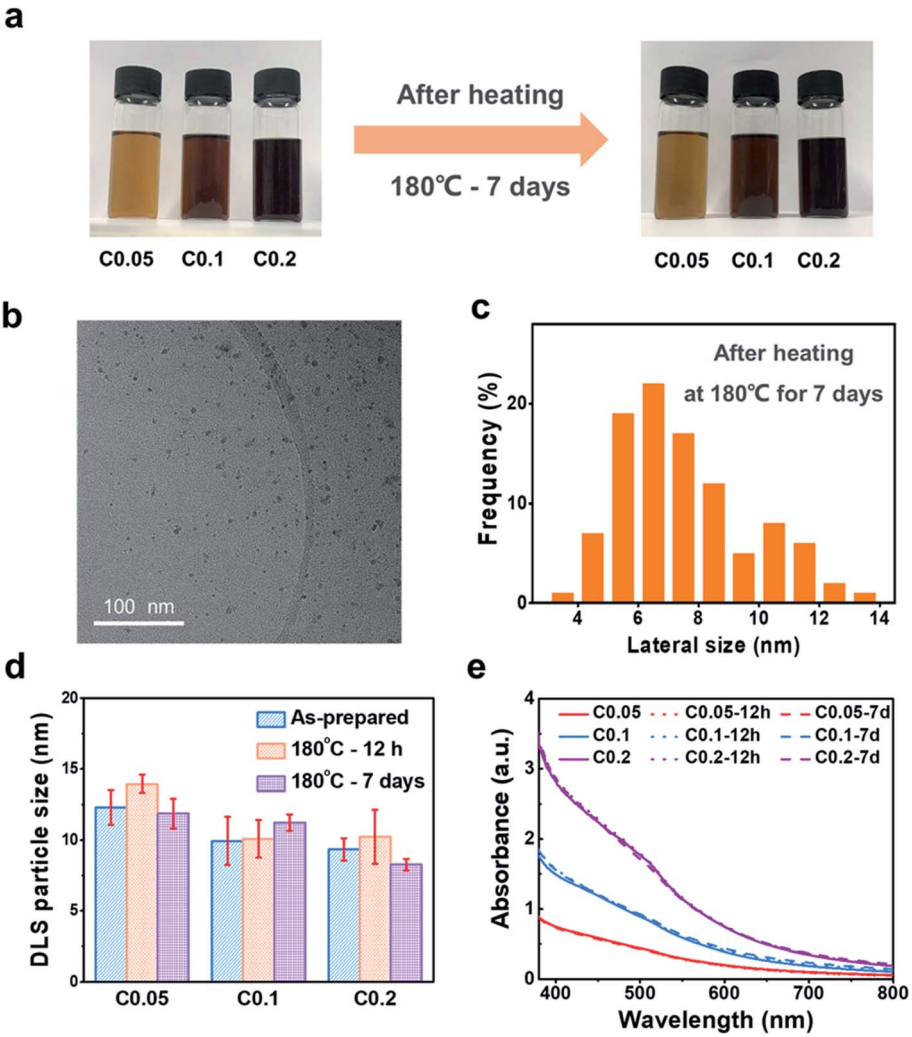

Fig. 3 Thermal stability test of GQD-EG nanofluids with different concentration after heating at 180 °C. (a) Photographs of GQD-EG nanofluids before and after heating for 7 days (from left to right: 0.2 mg mL^{-1}, 0.1 mg mL^{-1}, 0.05 mg mL^{-1}). (b) A TEM image of GQDs after heating for 7 days. (c) Particle size distribution histogram of GQDs after heating at 180 °C for 7 days. (d) Particle size of GQDs measured by DLS before and after heating. (e) Optical absorption spectra of GQD-EG nanofluids before and after heating.

the attractive interaction and repulsive interaction between the GQDs. According to the classical DLVO theory, two neighboring GQDs in nanofluids can be treated as two parallel plates with a separation distance of D (Fig. S3†), and the van der Waals attraction energy per unit area between two parallel flat plates of fixed thickness (L) can be estimated by:[44]

$$W_{\mathrm{vdW}} = -\frac{A_{\mathrm{H}}}{12\pi}\left[\frac{1}{D^2} - \frac{2}{(D+L)^2} + \frac{1}{(D+2L)^2}\right]$$

where A_{H} is the Hamaker constant. Compared with conventional graphene oxide (GO) or graphene sheets that have lateral sizes of several micrometers,[45,46] the small lateral size of the GQDs (~8 nm) signficantly weaks the interplane van der Waals attraction. As evidenced by the zeta potential measurement, the surfaces of GQDs are negatively charged due to the ionization and dissociation of surface groups, which can provide the repulsive force to counterbalance the van der Waals attraction and thus mitigate the aggregation tendency (Fig. S4†). However, detailed calculation and estimation indicate that the total DLVO interaction for the contacting GQDs is less than $k_{\mathrm{B}}T$, which is not sufficient to stabilize the GQDs in the nanofluids (Table S3†). Besides the DLVO interaction, the hydrogen bonding between OH-GQDs and EG provides the solvation force to prevent direct contact between GQDs. Herein, the interaction energy for the hydrogen bonding is estimated to be 21 kJ mol^{-1}, which means breaking each hydrogen bonding requires an energy input of ~$8.48k_{\mathrm{B}}T$ at room temperature.[47] This large energy barrier prevents the direct contact between GQDs and ensures their uniform dispersion within EG fluids.

Another requirement for achieving long-term stable dispersion is that the sedimentation of GQDs can be counterbalanced by the Brownian motion. For single GQD, the sedimentation velocity (V) in the nanofluids can be estimated by the Stokes law:[48]

$$V = \frac{d^2}{18\eta}(\rho_{\mathrm{P}} - \rho_{\mathrm{BF}})g$$

where ρ_P and ρ_{BF} are the densities of dispersed particles (2.25 g cm^{-3}) and base fluid (1.11 g cm^{-3}), η is the viscosity of fluid, g is the gravitational acceleration and d is the diameter of the particle. Considering that the sedimentation velocity is proportional to the square of particle size, smaller particles will significantly lower the sedimentation velocity (Fig. S5†). On the contrary, the thermal Brownian motion velocity is inversely proportional to the particle size.[49] Calculation shows that the small size of the GQDs enables a higher Brownian motion velocity than the sedimentation velocity, thus the dispersed GQDs can maintain their long-term stable dispersion within EG.

Thermophysical properties of nanofluids

Besides the stable uniform dispersion, high-performance nanofluids for direct solar energy harvesting should have broad light absorption, large heat capacity and low viscosity. The transmittance spectra of GQD-EG nanofluids in Fig. 4a shows that unlike the EG base fluid that is highly transparent, the transmittance quickly decreases with the increasing loading of OH-GQDs. By increasing the concentration to 0.2 mg mL^{-1}, transmittance of nanofluids is less than 10% in the visible region (380–760 nm). To evaluate the absorption performance of the nanofluids, the percentage of solar energy absorbed by the nanofluids (F) is calculated by:[50]

$$F = \frac{\int_{\lambda_{min}}^{\lambda_{max}} I(\lambda)\left(1 - e^{-\alpha(\lambda)x}\right)d\lambda}{\int_{\lambda_{min}}^{\lambda_{max}} I(\lambda)d\lambda}$$

where $I(\lambda)$ is the spectrum solar irradiance, $\alpha(\lambda)$ is the extinction coefficient, x is the penetration depth of sunlight, λ_{max} and λ_{min} are the maximum and minimum wavelength of the solar spectrum, respectively. The extinction coefficient was calculated by the Beer–Lambert Law: $\alpha(\lambda) = -\frac{1}{l}\ln T(\lambda)$, where l is the penetration distance (1 cm) and $T(\lambda)$ is the transmittance of nanofluids. Fig. 4b exhibits that over 90% of incident solar energy is absorbed by the 0.2 mg mL^{-1} GQD-EG nanofluids when the penetration depth is 3 cm. The low concentration in turn minimizes the influence of GQDs on the heat capacity and viscosity of the solar-thermal fluids. Fig. 4c shows the temperature-dependent specific heat capacity curves of the GQD-EG nanofluids are nearly overlapped with the curve of the neat EG. The effective specific heat capacity of the GQD-EG nanofluids can be estimated by:[51]

$$c_{p,NF} = \frac{\varphi\rho_P c_{p,P} + (1-\varphi)\rho_{BF} c_{p,BF}}{\varphi\rho_P + (1-\varphi)\rho_{BF}}$$

where ρ is the density and φ is the volume fraction of GQDs. The densities of GQDs and EG are estimated to be 1.8 g cm^{-3} and 1.11 g cm^{-3}, respectively.[52] The specific heat capacity of GQDs and EG are estimated to be 0.7 J g^{-1} K^{-1} and 2.5 J g^{-1} K^{-1} at room temperature. For the 0.2 mg mL^{-1} GQD-EG nanofluids, the calculated specific heat is only 0.013% lower than that of pure EG. Similarly, Fig. 4d presents that the difference in temperature-dependent viscosity is also negligible for the pure

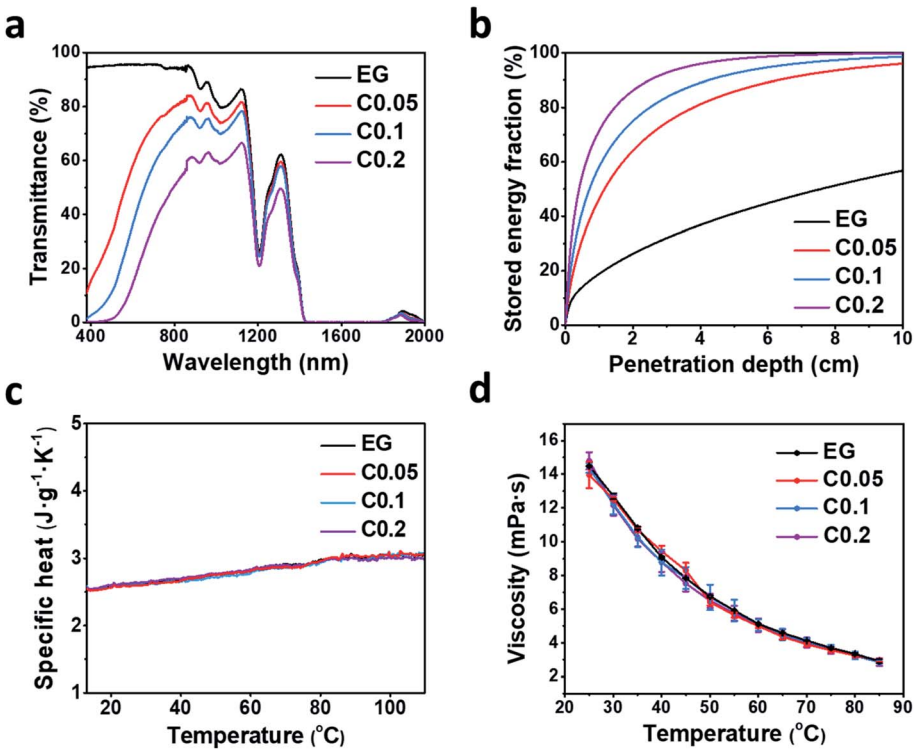

Fig. 4 (a) Transmittance spectra of EG and GQD-EG nanofluids with different concentration. (b) Store solar energy fraction as a function of the penetration depth of EG and GQD-EG nanofluids. (c) Specific heat capacity of EG and GQD-EG nanofluids *versus* temperature. (d) Viscosity of EG and GQD-EG nanofluids *versus* temperature.

EG and the GQD-EG nanofluids. Empirically, the viscosity of GQD-EG nanofluids (η) can be calculated by:[53]

$$\eta = \eta_0(1 + 2.5\varphi)$$

where η_0 is the viscosity of the base fluid. The calculated viscosity of the 0.2 mg mL^{-1} GQD-EG nanofluids is only 0.03% higher than pure EG. We also measured the thermal conductivity of EG and GQD-EG nanofluids at room temperature. As shown in Table S4,† the thermal conductivity slightly increased from 268.2 ± 0.9 mW m^{-1} K^{-1} for pure EG to 274.5 ± 2.9 mW m^{-1} K^{-1} for the 0.2 mg mL^{-1} GQD-EG nanofluids.

Direct absorption-based solar-thermal energy harvesting

With combined stable dispersion, high solar absorptance, large heat capacity and low viscosity, the GQD-EG nanofluids were used for medium-temperature direct absorption-based solar-thermal energy harvesting. The GQD-EG nanofluids were placed within a plastic cup wrapped by a PDMS thermal insulation layer and the whole setup was illuminated under concentrated solar fluxes generated by a solar simulator (Fig. 5a). Three thermocouples were employed to monitor the temperature evolution of the nanofluids at top, middle and bottom position and the average values were plotted. Fig. 5b shows that under 2-sun solar illumination (2 kW m^{-2}) for 30 min both EG and GQD-EG nanofluids (10 mL) are heated up and the maximum heating temperature increases with the loading of GQDs. Enhanced solar-thermal harvesting performance with the increasing loading of GQDs is clearly shown by comparing the temperature rise for GQD-EG nanofluids under solar illumination for 30 min (Fig. S6†). Under the same illumination condition, increasing the loading of GQDs from 0.05 mg mL^{-1} to 0.2 mg mL^{-1} the nanofluids were heated from 30 °C to 64.9 °C and 77.1 °C, respectively. It can be seen that high loading of GQDs helps increasing the stabilized heating temperature of the nanofluids. However, it should be noted that if the loading of photothermal converters is too high the solar-thermal conversion would only occur within the top surface layer of the nanofluids. The optimum loading of GQDs can fully absorb all the incident solar photons within the given height of the nanofluids such that the nanofluids are volumetrically and homogenously heated. With the same loading of GQDs (0.2 mg mL^{-1}), increasing solar fluxes can induce more intensive heating. Fig. 5c shows that by increasing the solar flux to 8 sun the GQD-EG nanofluids can be heated up to more than 170 °C.

Based on the measured temperature profiles, the solar-thermal harvesting efficiency of EG and GQD-EG nanofluids was calculated by:[45]

$$\eta = \frac{\text{stored thermal energy}}{\text{incident solar energy}} = \frac{\int_{T_i}^{T_f} mc_p(T)\mathrm{d}T}{Q_{\text{incident}}}$$

where m is the mass of the nanofluids, $c_p(T)$ is the specific heat capacity, T_i and T_f are the initial and final temperature of the nanofluids. Fig. S7a† shows that compared with the EG base fluids the addition of a minute amount of GQDs can significantly improve the solar-thermal harvesting efficiency. In the meanwhile, it was found that the solar-thermal harvesting efficiency gradually decreases with rising temperature of the nanofluids. For the 0.2 mg mL^{-1} GQD-EG nanofluids under 8

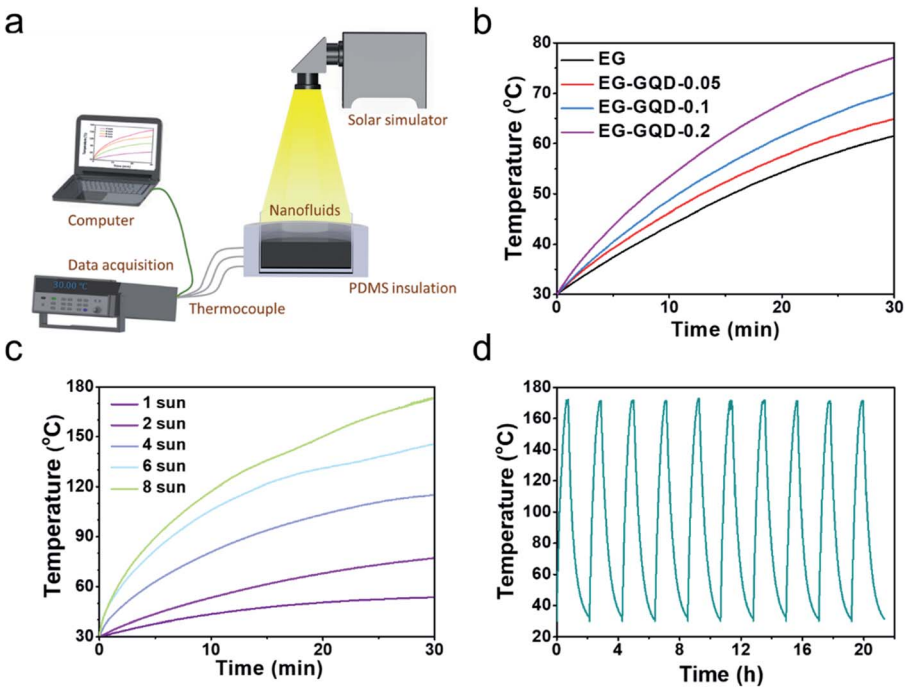

Fig. 5 (a) Schematic experimental setup for direct absorption-based solar-thermal energy harvesting with GQD-EG nanofluids. (b) Temperature evolution profiles of GQD-EG nanofluids with different concentration of GQDs under 2 sun solar illumination (2 kW m^{-2}) for 30 min. (c) Temperature evolution profiles of GQD-EG nanofluids (0.2 mg mL^{-1}) under solar illumination with different intensity for 30 min. (d) Cycled heating/cooling tests of GQD-EG nanofluids (0.2 mg mL^{-1}) under 7 kW m^{-2} solar illumination for 36 min and natural cooling down for 90 min.

sun solar illumination, the solar-thermal harvesting efficiency dropped from 97% at 30 °C to 16% when the nanofluids were heated 170 °C (Fig. S7b†). The decreased efficiency should be attributed to the increased heat losses from the nanofluid system. As shown by the energy balance scheme of the DASC (Fig. S8†), besides the solar-thermal energy stored within the nanofluids, part of the incident solar energy is lost through heat conduction, heat convection, heat radiation, evaporation of base fluids, and light reflection and transmission.[54] Specifically, the harvested heat in the nanofluids can be conducted through the beaker to heat up the PDMS layer. The overall nanofluid device can also lose heat through radiation and convection from the top surface. It was also noted that with rising temperature of the nanofluids evaporation of the EG base fluid became pronounced. In particular, when the operating temperature of the nanofluids was higher than 140 °C, the evaporation loss of EG was serious and the large evaporation enthalpy of EG would lower the amount of heat harvested in the nanofluids. Additionally, part of the incident sunlight is reflected at the top surface. If the incident solar photons are not fully absorbed by the nanofluids, the transmission loss could occur from the bottom of nanofluid container. In practical applications, the nanofluids can be sealed within confined systems with an extremely low thermal conductivity to suppress the various forms of heat losses. Moreover, the ideal concentration of photothermal converters and the height of the nanofluids should be identified so that all the incident solar photons can be captured by the nanofluids within the DASCs. With the improved system design and the optimum combination of concentration and height of GQD-EG nanofluids, consistent high solar-thermal harvesting efficiency can be expected within a broad range of operation temperatures.

To test the cycling performance, the 0.2 mg mL^{-1} GQD-EG nanofluids were exposed to repeated heating/cooling cycles through direct solar illumination with a power density of 7 kW m^{-2} for 36 min followed by naturally cooling for 90 min. Fig. 5d shows that the fluids reached a maximum temperature around 170 °C and then cooled down to 30 °C, and the heating/cooling temperature profiles remain largely same during the tests for 10 cycles, which should be attributed to the stable dispersion and consistent thermophysical properties of the GQD-EG nanofluids.

Conclusions

To summarize, this work demonstrated a facile way to prepare stably-dispersed GQD-EG nanofluids for direct absorption-based solar energy harvesting at medium temperatures. Instead of resorting to complicated surface modification methods, this work synthesized small-sized OH-GQDs as the self-dispersible solar absorber and capitalized on the hydrogen bonding interaction between the surface of OH-GQDs and EG fluids to achieve long-term stable dispersion. Dispersion stability tests indicated that the GQD-EG nanofluids could maintain their uniform dispersion after continuous heating at 180 °C for 7 days. The prepared GQD-EG nanofluids also exhibited other desired attributes for solar-thermal energy harvesting such as broadband sunlight absorption, high specific heat capacity and low viscosity. The stably dispersed GQD-EG nanofluids have been successfully used for reliable, consistent, volumetric solar-thermal energy harvesting under direct illumination of concentrated solar illumination with a heating temperature up to 170 °C. It is anticipated that the reported stably-dispersed carbon nanofluids would not only expand the application of GQDs into solar-thermal fields but also boost the exploration of nanofluid technologies that involve elevated operation temperatures.

Conflicts of interest

There are no conflicts to declare.

Acknowledgements

The authors thank the financial support from National Key R&D Program of China (2017YFB0406100), National Natural Science Foundation of China (51873105), Shanghai Rising-Star Program (18QA1402200), Innovation Program of Shanghai Municipal Education Commission (2019-01-07-00-02-E00069) and the funding from Center of Hydrogen Science, Shanghai Jiao Tong University.

References

1 Y. Tian and C. Y. Zhao, *Appl. Energy*, 2013, **104**, 538–553.
2 Z. Wang, A. Roffey, R. Losantos, A. Lennartson, M. Jevric, A. U. Petersen, M. Quant, A. Dreos, X. Wen, D. Sampedro, K. Börjesson and K. Moth-Poulsen, *Energy Environ. Sci.*, 2019, **12**, 187–193.
3 P. Tao, G. Ni, C. Song, W. Shang, J. Wu, J. Zhu, G. Chen and T. Deng, *Nat. Energy*, 2018, **3**, 1031–1041.
4 Y. Zhang, T. Xiong, D. K. Nandakumar and S. C. Tan, *Adv. Sci.*, 2020, **7**, 1903478.
5 Y. Zhang, T. Xiong, L. Suresh, H. Qu, X. Zhang, Q. Zhang, J. Yang and S. C. Tan, *ACS Energy Lett.*, 2020, **5**, 3397–3404.
6 J. Xu, Z. Wang, C. Chang, B. Fu, P. Tao, C. Song, W. Shang and T. Deng, *Desalination*, 2020, **484**, 114423.
7 J. Xu, J. Zhang, B. Fu, C. Song, W. Shang, P. Tao and T. Deng, *ACS Appl. Mater. Interfaces*, 2020, **12**, 47612–47622.
8 P. Tao, C. Chang, Z. Tong, H. Bao, C. Song, J. Wu, W. Shang and T. Deng, *Energy Environ. Sci.*, 2019, **12**, 1613–1621.
9 Q. Ye, P. Tao, C. Chang, L. Zhou, X. Zeng, C. Song, W. Shang, J. Wu and T. Deng, *ACS Appl. Mater. Interfaces*, 2018, **11**, 3417–3427.
10 C. Chang, X. Nie, X. Li, P. Tao, B. Fu, Z. Wang, J. Xu, Q. Ye, J. Zhang, C. Song and W. Shang, *J. Mater. Chem. A*, 2020, **8**, 20970–20978.
11 X. Chen, H. Gao, Z. Tang, W. Dong, A. Li and G. Wang, *Energy Environ. Sci.*, 2020, **13**, 4498–4535.
12 X. Li, J. Zhang, B. Fu, C. Song, W. Shang, P. Tao and T. Deng, *Energy Convers. Manage.*, 2020, **222**, 113241.
13 Y. Zhang, S. K. Ravi and S. C. Tan, *Nano Energy*, 2019, **65**, 104006.
14 T. P. Otanicar, P. E. Phelan, R. S. Prasher, G. Rosengarten and R. A. Taylor, *J. Renewable Sustainable Energy*, 2010, **2**, 033102.

15 A. Lenert and E. N. Wang, *Sol. Energy*, 2012, **86**, 253–265.
16 T. B. Gorji and A. A. Ranjbar, *Renewable Sustainable Energy Rev.*, 2017, **72**, 10–32.
17 E. Sani, N. Papi, L. Mercatelli and G. Zyla, *Renewable Energy*, 2018, **126**, 692–698.
18 W. Chen, C. Zou and X. Li, *Sol. Energy Mater. Sol. Cells*, 2019, **200**, 109931.
19 X. Li, W. Chen and C. Zou, *Sol. Energy Mater. Sol. Cells*, 2020, **204**, 110240.
20 M. Vakili, S. M. Hosseinalipour, S. Delfani, S. Khosrojerdi and M. Karami, *Sol. Energy*, 2016, **131**, 119–130.
21 F. Yu, Y. Y. Chen, X. B. Liang, J. L. Xu, C. S. Lee, Q. Liang, P. Tao and T. Deng, *Prog. Nat. Sci.*, 2017, **27**, 531–542.
22 B. Fu, J. Zhang, H. Chen, H. Guo, C. Song, W. Shang, P. Tao and T. Deng, *Curr. Opin. Chem. Eng.*, 2019, **25**, 51–56.
23 Y. Y. Chen, X. J. Quan, Z. Y. Wang, C. S. Lee, Z. Z. Wang, P. Tao, C. Y. Song, J. B. Wu, W. Shang and T. Deng, *J. Mater. Chem. A*, 2016, **4**, 17503–17511.
24 J. Navas, P. Martinez-Merino, A. Sanchez-Coronilla, J. J. Gallardo, R. Alcantara, E. I. Martin, J. C. Pinero, J. R. Leon, T. Aguilar, J. H. Toledo and C. Fernandez-Lorenzo, *J. Mater. Chem. A*, 2018, **6**, 14919–14929.
25 P. Tian, L. Tang, K. S. Teng and S. P. Lau, *Mater. Today Chem.*, 2018, **10**, 221–258.
26 F. Zhang, F. Liu, C. Wang, X. Xin, J. Liu, S. Guo and J. Zhang, *ACS Appl. Mater. Interfaces*, 2016, **8**, 2104.
27 B. Trauzettel, D. V. Bulaev, D. Loss and G. Burkard, *Nat. Phys.*, 2007, **3**, 192.
28 L. Tang, R. Ji, X. Cao, J. Lin, H. Jiang, X. Li, K. S. Teng, C. M. Luk, S. Zeng, J. Hao and S. P. Lau, *ACS Nano*, 2012, **6**, 5102.
29 K. A. Ritter and J. W. Lyding, *Nat. Mater.*, 2009, **8**, 235–242.
30 X. T. Zheng, A. Ananthanarayanan, K. Q. Luo and P. Chen, *Small*, 2015, **11**, 1620–1636.
31 A. El Fatimy, R. L. Myers-Ward, A. K. Boyd, K. M. Daniels, D. K. Gaskill and P. Barbara, *Nat. Nanotechnol.*, 2016, **11**, 335–338.
32 D. I. Son, B. W. Kwon, D. H. Park, W.-S. Seo, Y. Yi, B. Angadi, C.-L. Lee and W. K. Choi, *Nat. Nanotechnol.*, 2012, **7**, 465–471.
33 T. Van Tam, S. G. Kang, K. F. Babu, E. S. Oh, S. G. Lee and W. M. Choi, *J. Mater. Chem. A*, 2017, **5**, 10537–10543.
34 Z. Zhang, J. Zhang, N. Chen and L. Qu, *Energy Environ. Sci.*, 2012, **5**, 8869–8890.
35 J. Ge, M. Lan, B. Zhou, W. Liu, L. Guo, H. Wang, Q. Jia, G. Niu, X. Huang, H. Zhou, X. Meng, P. Wang, C.-S. Lee, W. Zhang and X. Han, *Nat. Commun.*, 2014, **5**, 4596.
36 X. Li, M. Rui, J. Song, Z. Shen and H. Zeng, *Adv. Funct. Mater.*, 2015, **25**, 4929.
37 Y. Yan, J. Gong, J. Chen, Z. Zeng, W. Huang, K. Pu, J. Liu and P. Chen, *Adv. Mater.*, 2019, **28**, 1808283.
38 H. Tetsuka, A. Nagoya, T. Fukusumi and T. Matsui, *Adv. Mater.*, 2016, **28**, 4632–4638.
39 Y. Yan, J. Chen, N. Li, J. Tian, K. Li, J. Jiang, J. Liu, Q. Tian and P. Chen, *ACS Nano*, 2018, **12**, 3523.
40 L. Wang, Y. Wang, T. Xu, H. Liao, C. Yao, Y. Liu, Z. Li, Z. Chen, D. Pan, L. Sun and M. Wu, *Nat. Commun.*, 2014, **5**, 5357.
41 X. W. Wang, G. Z. Sun, N. Li and P. Chen, *Chem. Soc. Rev.*, 2016, **45**, 2239–2262.
42 D. Pan, J. Zhang, Z. Li and M. Wu, *Adv. Mater.*, 2010, **22**, 734–738.
43 B. Sun, Z. Dreger and Y. Gupta, *J. Phys. Chem. A*, 2008, **112**, 10546–10551.
44 V. A. Parsegian, *van der Waals Forces: a Handbook for Biologists, Chemists, Engineers, and Physicists*, Cambridge University Press, New York, 2005.
45 L. Shu, J. Y. Zhang, B. W. Fu, J. L. Xu, P. Tao, C. Y. Song, W. Shang, J. B. Wu and T. Deng, *RSC Adv.*, 2019, **9**, 12082–12088.
46 L. Dong, Z. Chen, X. Zhao, J. Ma, S. Lin, M. Li, Y. Bao, L. Chu, K. Leng, H. Lu and K. P. Loh, *Nat. Commun.*, 2018, **9**, 76.
47 K. Wendler, J. Thar, S. Zahn and B. Kirchner, *J. Phys. Chem. A*, 2010, **114**, 9529–9536.
48 E. Lee, J. Ryu and J. Jang, *Chem. Commun.*, 2013, **49**, 9995–9997.
49 S. P. Jang and S. U. Choi, *Appl. Phys. Lett.*, 2004, **84**, 4316–4318.
50 E. Sani, S. Barison, C. Pagura, L. Mercatelli, P. Sansoni, D. Fontani, D. Jafrancesco and F. Francini, *Opt. Express*, 2010, **18**, 5179–5187.
51 S. Q. Zhou and R. Ni, *Appl. Phys. Lett.*, 2008, **92**, 093123.
52 F. Sedaghat, F. Yousefi and H. Zolfaghari, *J. Eng. Thermophys.*, 2019, **28**, 276–290.
53 M. K. Abdolbaqi, N. A. C. Sidik, A. Aziz, R. Mamat, W. H. Azmi, M. N. A. W. M. Yazid and G. Najafi, *Int. Commun. Heat Mass Transfer*, 2016, **77**, 22–32.
54 G. Ni, N. Miljkovic, H. Ghasemi, X. Huang, S. V. Boriskina, C.-T. Lin, J. Wang, Y. Xu, M. M. Rahman, T. Zhang and G. Chen, *Nano Energy*, 2015, **17**, 290–301.

